17th Brazilian Congress of Thermal Sciences and Engineering
November 25th-28th, 2018, Águas de Lindóia, SP, Brazil

ENCIT-2018-0219
SU² CFD SIMULATION OF THE HYPERSONIC TECHNOLOGICAL DEMONSTRATOR 14-X B AT FLIGHT MACH NUMBER 7

Mateus Santos de Paula Vieira
Leo Sperandio Dias Gonçalves
Universidade do Vale do Paraíba – UNIVAP. Av. Shishima Hifumi, 2911, Urbanova, CEP 12.224-000 - São José dos Campos – SP, Brasil
mateusdepaulavieira@live.com
leosperandio@gmail.com

Paulo Gilberto de Paula Toro
Universidade Federal do Rio Grande do Norte – UFRN, CT de Tecnologia. Senador Salgado Filho, 3000 - Campus Universitário, Lagoa Nova, CEP 59.078-970 – Natal – RN, Brasil.
toro@ct.ufrn.br

Heidi Korzenowski
Universidade do Vale do Paraíba – UNIVAP. Av. Shishima Hifumi, 2911, Urbanova, CEP 12.224-000 - São José dos Campos – SP, Brasil
heidi@univap.br

Israel da Silveira Rego
Instituto de Estudos Avançados – IEAv. Trevo Coronel Aviador José Alberto Albano do Amarante, 1, Putim, CEP 12.228-001 - São José dos Campos – SP, Brasil.
israel.rego@ieav.cta.br

Abstract. *The SCRamjet 14-X B vehicle aims to demonstrate the hypersonic airbreathing propulsion technology based on supersonic combustion, and it is designed to fly in the Earth's atmosphere at an altitude of 30 km and at the speed corresponding to Mach number 7. This work uses the computational software "SU² CFD" to analyze the behavior of the air flow along the 14-X B vehicle flying under the design conditions. Non-viscous (no boundary layer) effect, calorically gas perfect behavior (with no real gas effects) and disregarding hydrogen burning is considered. Theoretical analysis and numerical simulation via CFD are obtained for the thermodynamic properties along the vehicle and both are compared.*

Keywords: *Propulsion, SCRamjet, Aerothermodynamics, Hypersonic.*

1. INTRODUCTION

The SCRamjet 14-X B Technological Demonstrator consists of the compression section, combustion section and expansion section; designed to fly at the speed corresponding to Mach number 7 at 30 km altitude. Knowing the atmospheric conditions at the flight altitude as pressure, density and temperature one can analyzed the flow behavior at the vehicle air inlet, where positive deflection compression ramps are added. The plane oblique shock waves are established at the deflection ramps and are responsible for decelerating the flow to supersonic velocity and alter the thermodynamic properties at the combustion chamber, to ensure the autoignition and efficient burning of the hydrogen added to the supersonic air flow in the combustion chamber. Subsequently the flow leaves the combustion chamber passes through the expansion section, where the flow passes through negative deflection ramp and a expansion wave is established, where the flow is accelerated to ensure the necessary thrust in order to produce hypersonic flight.

2. METHODOLOGY

Before starting the calculations and simulations, the undisturbed flow located ahead of the vehicle, called freestream, is considered to the present study. It is comprised, by the compression section, the values of the thermodynamic properties in the Earth's atmosphere at the flight level of the vehicle.

2.1 Theoretical foundation and mathematical equations

The oblique shock wave theory relates the flow through the shock wave. After the oblique shock wave the flow decelerates but compress the airflow to higher pressure, temperature and density. The oblique shock wave also changes the direction of the flow, parallel to the surface of the ramp as shows the Fig 1, but remains supersonic.

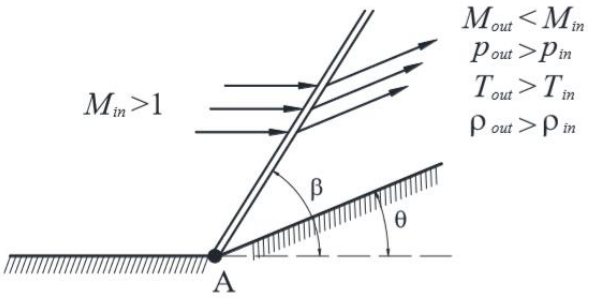

Figure 1. Properties through the Oblique Shock Wave (ANDERSON, 2003).

At the moment the flow meets a deflection an incident oblique shock wave is established, the velocity corresponding to the Mach number of the flow can be decomposed into two components, tangential and perpendicular to the shock wave as shown in the Fig 2.

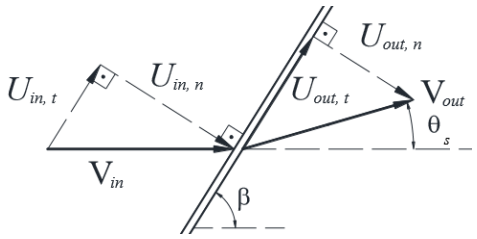

Figure 2. Flow through the Shock Wave Incident (ANDERSON, 2003).

The tangential velocity remains the same before and after the incident oblique shock wave as shown in Eq. (1). The subscript (t) refers to the tangential component.

$$u_{in,t} = u_{out,t} \tag{1}$$

Starting from the physical principles of Conservation (Continuity, Quantity of Motion and Energy), one can relate the flow behavior before and after the incident oblique shock wave considering the perpendicular velocity, or normal to the shock wave. In this way one can obtain through the oblique incident shock wave. The subscript (n) refers to the normal component. (CARVALHAL, 2015).

$$\rho_{in}\ u_{in,n} = \rho_{out}\ u_{out,n} \tag{2}$$

$$P_{in} + \rho_{in}\ u_{in,n}^2 = P_{out} + \rho_{out}\ u_{out,n}^2 \tag{3}$$

$$h_{in} + \frac{u_{in,n}^2}{2} = h_{out} + \frac{u_{out,n}^2}{2} \tag{4}$$

Manipulating mathematically the equations the ratios between the properties before (in) and after (out) of the oblique shock wave are obtained, considering is calorically perfect gas and there is no viscous effects (Anderson, 2003).

$$\frac{P_{out}}{P_{in}} = 1 + \frac{2\gamma}{(\gamma+1)}\left[\left(M_{in}\,sen\beta\right)^2 - 1\right] \tag{5}$$

$$\frac{\rho_{out}}{\rho_{in}} = \frac{\left[(\gamma+1)\left(M_{in}sen\beta\right)^2\right]}{\left[(\gamma-1)\left(M_{in}sen\beta\right)^2+2\right]} \tag{6}$$

$$\frac{T_{out}}{T_{in}} = \frac{P_{out}}{P_{in}}\frac{\rho_{in}}{\rho_{out}} \tag{7}$$

$$\frac{T_{out}}{T_{in}} = \left(1+\frac{2\gamma}{(\gamma+1)}\left[(M_{in}sen\beta)^2-1\right]\right)\left(\frac{(\gamma-1)(M_{in}sen\beta)^2+2}{(\gamma+1)(M_{in}sen\beta)^2}\right) \tag{7}$$

It is necessary to know the deflection angles (θ) and the angle of the incident shock wave (β). Analyzing the geometry presented in figure 2, one can obtain the relation θ-β-M.

$$\frac{tg\left(\beta-\theta_S\right)}{tg\beta} = \frac{u_{out,n}/u_{out,t}}{u_{in,n}/u_{in,t}} \tag{8}$$

Considering Eq. (1):

$$\frac{tg\left(\beta-\theta_S\right)}{tg\beta} = \frac{u_{out,n}}{u_{in,n}} \tag{9}$$

Also, considering the ratio between the specific mass (density) before and after the incident oblique shock wave, and doing some trigonometric manipulations, one arrives at the relation θ-β-M.

$$tg\theta_s = 2\left(\cot g\beta\right)\left[\frac{\left(M_{in}sen\beta\right)^2-1}{M_{in}^2\left(\gamma+\cos 2\beta\right)+2}\right] \tag{10}$$

Finally, the Mach number corresponding to the velocity of the flow after the oblique shock wave is found by Eq. (11), obtained after trigonometric manipulations between the deflection angles (θ), the angle of the incident shock wave (β) and the ratio between the specific masses before (in) and after (out) the oblique shock wave. (Anderson, 2003).

$$M_{out} = \frac{\sqrt{\dfrac{\left(M_{in}sen\beta\right)^2+\dfrac{2}{(\gamma-1)}}{\dfrac{2\gamma}{(\gamma-1)}\left(M_{in}sen\beta\right)^2-1}}}{sen(\beta-\theta_s)} \tag{11}$$

The Oblique Plane Reflected Shock Wave Theory addresses the behavior of the oblique shock wave upon finding a solid wall, where there will be reflection of the wave with angle (θ) equal to the angle of deflection that originated the incident oblique shock wave, but the wave of reflected shock has its own angle (β) since this is in function of θ and M_in. The current lines of the flow run through the incident and reflected shock waves, where it has its direction altered and after the reflected shock wave continue parallel to the surface (Fig. 3). (Anderson, 2003).

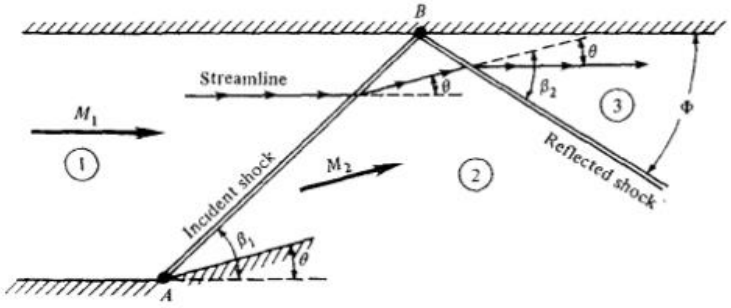

Figure 3. Reflected Shock Wave (ANDERSON, 2003).

The properties after the reflected shock wave can be found through the Eq (5), Eq. (6), Eq. (7) and Eq. (11), from the equations concerning the incident shock wave.

Contrary to the compression ramps, where the flow is decelerated, one can add expansion ramps, where the flow is accelerated according to the theory of expansion waves. Expansion waves occur when the flow at supersonic velocity or greater adjacent to a flat plate encounters a negative deflection and needs to adjust to keep close to the surface, this adjustment happens so that the flow forms an expansion fan that originates in the deflection, and through the fan the flow has its speed increased, but pressure, temperature and density decrease.

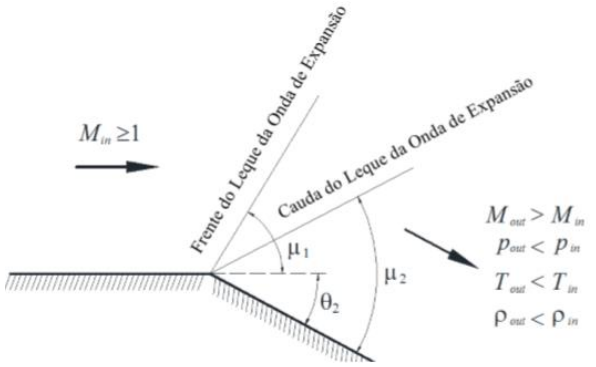

Figure 4. Theory of Expansion Wave (ANDERSON, 2003).

The Expansion Wave is limited by the Mach Waves on the front and the tail of the expansion fan, $\mu_{in} = \mu_1$ and $\mu_{out} = \mu_2$ respectively. They are defined by:

$$\mu_{in} = arcsen\left(\frac{1}{M_{in}}\right) \tag{12}$$

$$\mu_{out} = arcsen\left(\frac{1}{M_{out}}\right) \tag{13}$$

The angle is defined using the Prandtl-Meyer function υ:

$$\theta_2 = \upsilon(M_{out}) - \upsilon(M_{in}) \tag{14}$$

The Prandtl-Meyer function is defined by Eq. (15):

$$\upsilon(M) = \sqrt{\frac{\gamma+1}{\gamma-1}}\ tg^{-1}\sqrt{\frac{\gamma-1}{\gamma+1}(M^2+1)} - tg^{-1}\sqrt{M^2-1} \tag{15}$$

After discovering the Mach number after the expansion wave, the isentropic relationships given by equations (16), (17) and (18) can be used to determine the values of the thermodynamic properties after the expansion wave.

$$\frac{P_{out}}{P_{in}} = \left(\left(\frac{1+\frac{\gamma-1}{2}M_{in}^{2}}{1+\frac{\gamma-1}{2}M_{out}^{2}} \right) \right)^{\frac{\gamma}{\gamma-1}} \tag{16}$$

$$\frac{T_{out}}{T_{in}} = \left(\frac{1+\frac{\gamma-1}{2}M_{in}^{2}}{1+\frac{\gamma-1}{2}M_{out}^{2}} \right) \tag{17}$$

$$\frac{\rho_{out}}{\rho_{in}} = \frac{P_{out}}{P_{in}} \frac{T_{in}}{T_{out}} \tag{18}$$

2.2 List of characteristics of the atmosphere in the flight level

The characteristics of the terrestrial atmosphere in the flight level of the vehicle can be find on the book “US Standard Atmosphere 1976” of NASA, National Aeronautics and Space Administration of the United States of America.

Table 1. Properties of the terrestrial atmosphere at 30 km of altitude. (NASA)

Property	Unit	Value of property
Mach Number of flight	[-]	7
Temperature	[K]	226.5
Pressure	[Pa]	1197
Density	[kg/m³]	0.018410

2.3 Vehicle cross-section terminology

The 14-X B Technological Demonstrator can be divided into sections to make it easier to understand. In the study, the authors divided the vehicle into compression section, combustion section and expansion section. This can be observed by Fig 5.

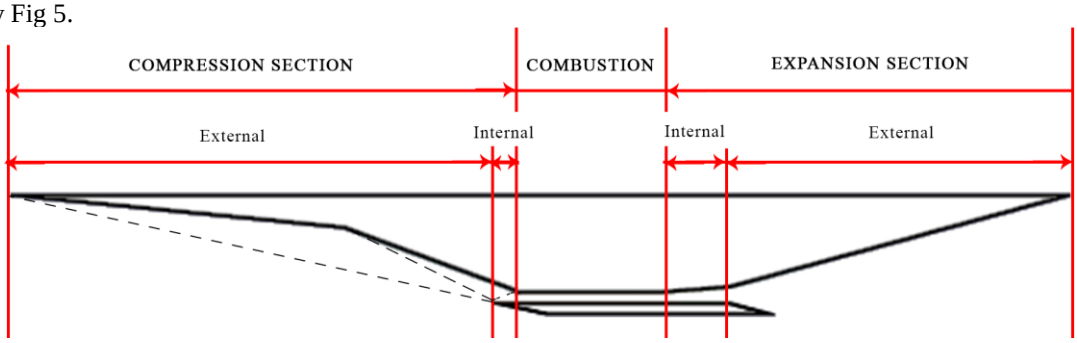

Figure 5. 14–X B Terminology (The Authors).

2.4 Theoretical-Analytical Analysis

The values of the flow properties of the air flow, that passes through the leading edge and goes to the combustion chamber entrance, can be obtained mathematically using the Oblique Shock Wave Theory and the Reflected Shock Wave Theory. The values of the flow properties of the air flow, that leave the combustion chamber and pass through the expansion section, can be obtained mathematically using the Expansion Wave Theory. These equations can also be developed via computer software for mathematical calculation.

In this work a computer code was developed by inserting the mathematical equation in the free software "Octave", similar to the software "MATLAB". The values of the same properties were also obtained using the software "HAP" (included in the book “Hypersonic Airbreathing Propulsion (Heiser and Pratt, 1994) and the appendices presented by the book "Modern compressible flow" (Anderson Junior, J. D., 2003).

To start the calculation, it was necessary to divide the vehicle again, this time in some subsections, adding the free flow before the vehicle and dividing the compression section in the two ramps that constitute it. The expansion section was also divided into the two ramps that comprise it. The subsections can be seen in Fig 6.

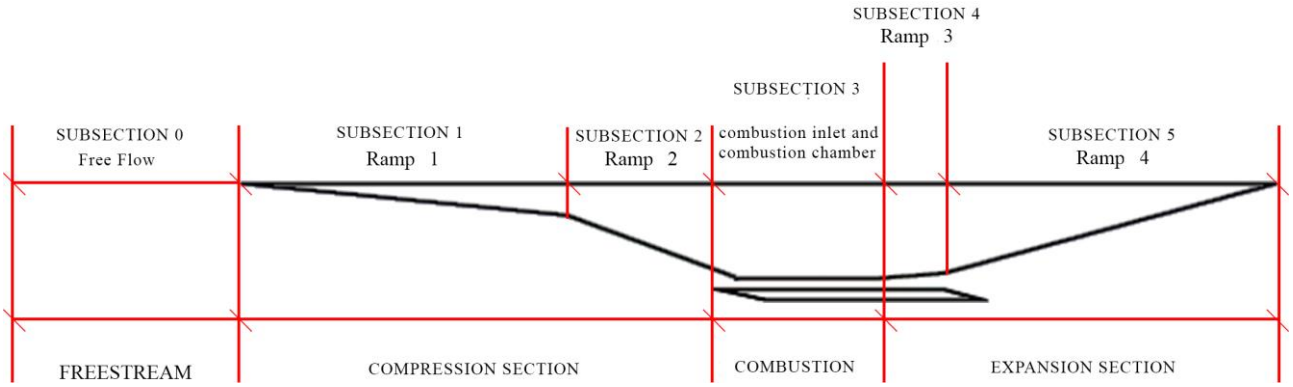

Figure 6. 14-X B Terminology with subsections (The Authors).

2.5 Theoretical-Numerical Simulation

In this work, the numerical simulation was divided into four stages. The first step concerns the generation of geometry, the second stage concerns the incorporation of geometry in the mesh generation software, in the third stage is written the computational code responsible for managing the computational fluid dynamics (CFD) simulation software, the last step is to execute the simulations in the software "SU²_CFD" and integrate the results obtained via CFD to a results visualization software.

Firstly, the geometry of the vehicle was designed in the software generator of unstructured meshes "GMSH". This geometry relies on the Farfield throughout the vehicle. The geometry and the distribution scheme of the initial conditions of the simulation can be seen in Fig (7), “Farfield” are the properties of the free flow around the vehicle, “Paredes (wall)” are the surface vehicle.

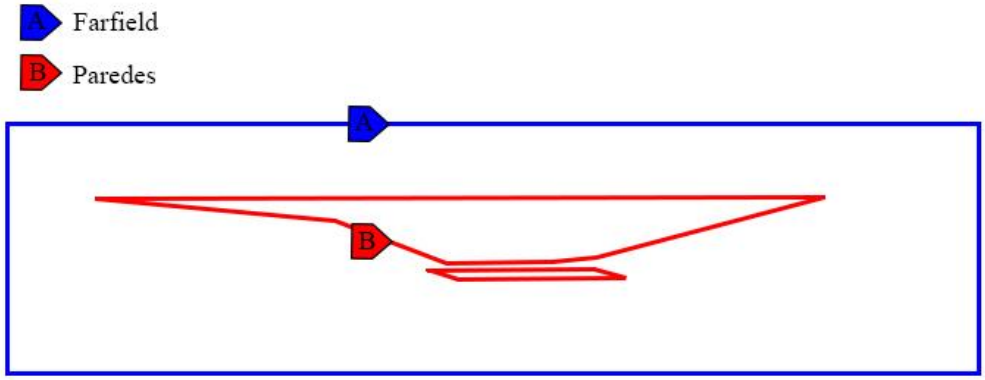

Figure 7. Physical modeling of the mesh in the "GMSH" software. (The Authors)

From the geometry, a mesh with 396 thousand triangles was generated. This mesh is a text file that is implemented at the code of the software SU², and executed in the Command Prompt of the computer, the code promotes the solution of the Euler equations around the mesh, solving the flow and obtaining the thermodynamic properties throughout the vehicle.

3. RESULTS AND DISCUSSIONS

3.1 Results of Theoretical-Numerical Analysis.

The values of the thermodynamic properties and the Mach number along the vehicle are analyzed analytically by software "HAP", through software "Octave" and also in handwritten form. The results are judged to be more consistent,

the "Octave" results and those obtained handwritten have a low percentage error in relation to "HAP" results. The results presented are presented in the following tables 2 to 4:

Table 2. Thermodynamic properties and Mach number along the Technological Demonstrator 14-X B flying under the design conditions. Results by HAP.

-		Freestream	Compression section		Combustion	Expansion section	
Property	Unit	Subsection 0	Subsection 1	Subsection 2	Subsection 3	Subsection 4	Subsection 5
-	-	Freestream	Ramp 1 5.5°	Ramp 2 14.5°	Combustor and Combustor Intake	Ramp 3 4.27°	Ramp 4 10.73º
M_{in}	[-]	7	7	6.0188	4.0645	2.6012	2.7981
Θ_{in}	[°]	-	5.5	14.5	20	4.27	10.73
β_{out}	[°]	-	12.243	22.114	32.238	-	-
M_{out}	[-]	-	6.0188	4.0645	2.6012	2.7981	3.3715
T_{out}	[K]	226.5	296.692	568.374	1039.555	953.272	747.175
P_{out}	[Pa]	1197	2877.59	16755.91	89104.56	65803.72	28052.13
ρ_{out}	[kg/m³]	0.018410	0.033788	0.102702	0.298605	0.240467	0.130953
a_{out}	[m/s]	301.6748	345.2694	477.8833	646.2919	618.8899	547.9186
u_{out}	[m/s]	2111.7238	2078.1077	1942.3568	1681.1346	1731.7159	1847.3075
μ_1	[°]	-	-	-	-	22.6107	20.9405
μ_2	[°]	-	-	-	-	20.939	17.2536

Table 3. Thermodynamic properties and Mach number along the Technological Demonstrator 14-X B flying under the design conditions. Results by software Octave.

–		Freestream	Compression section		Combustion	Expansion section	
Property	Unit	Subsection 0	Subsection 1	Subsection 2	Subsection 3	Subsection 4	Subsection 5
–	–	Freestream	Ramp 1 5.5°	Ramp 2 14.5°	Combustor and Combustor Intake	Ramp 3 4.27°	Ramp 4 10.73º
M_{in}	[-]	7	7	6.0224 ± 0.060%	4.0629 ± 0.040%	2.6016 ± 0.015%	2.8214 ± 0.833%
Θ_{in}	[°]	–	5.5	14.5	20	4.27	10.73
β_{out}	[°]	–	12.240 ± 0.025%	22.115 ± 0.003%	32.239 ± 0.002%	–	–
M_{out}	[-]	–	6.0224 ± 0.060%	4.0629 ± 0.040%	2.6016 ± 0.015%	2.8214 ± 0.833%	3.4003 ± 0.854%
T_{out}	[K]	226.5	296.630 ± 0.021%	568.620 ± 0.043%	1039.580 ± 0.002%	943.968 ± 0.976%	738.684 ± 1.136%
P_{out}	[Pa]	1197	2876.16 ± 0.050%	16769.10 ± 0.079%	89105.07 ± 0.001%	63569.72 ± 3.395%	26949.66 ± 3.930%
ρ_{out}	[kg/m³]	0.018410	0.034000 ± 0.628%	0.102733 ± 0.031%	0.298582 ± 0.008%	0.24263 ± 0.900%	0.128487 ± 1.883%
a_{out}	[m/s]	301.6748	345.2300 ± 0.011%	477.8684 ± 0.003%	646.3020 ± 0.003%	615.86223 ± 0.489%	544.7964 ± 0.570%
u_{out}	[m/s]	2111.7238	2079.1299 ± 0.049%	1941.5201 ± 0.043%	1681.4186 ± 0.017%	1737.5939 ± 0.339%	1852.4711 ± 0.280%
μ_1	[°]	–	–	–	–	22.6052 ± 0.024%	20.7588 ± 0.868%
μ_2	[°]	–	–	–	–	20.79 ± 0.864%	17.1031 ± 0.872%

Table 4. Thermodynamic properties and Mach number along the Technological Demonstrator 14-X B flying under the design conditions. Calculations manually.

-		Freestream	Compression section		Combustion	Expansion section	
Property	Unit	Subsection 0	Subsection 1	Subsection 2	Subsection 3	Subsection 4	Subsection 5
-	-	Freestream	Ramp 1 5.5°	Ramp 2 14.5°	Combustor and Combustor Intake	Ramp 3 4.27°	Ramp 4 10.73º
M_{in}	[-]	7	7	6.035 ± 0.269%	4.033 ± 0.775%	2.613 ± 0.454%	2.8 ± 0.068%
Θ_{in}	[°]	-	5.5	14.5	20	4.27	10.73
β_{out}	[°]	-	12.24 ± 0.025%	23 ± 4.005%	32.4 ± 0.501%	-	-
M_{out}	[-]	-	6.035 ± 0.269%	4.033 ± 0.775%	2.613 ± 0.454%	2.8 ± 0.068%	3.4 ± 0.845%
T_{out}	[K]	226.5	296.04 ± 0.200%	576.39 ± 1.410%	1044.99 ± 0.523%	957.1 ± 0.402%	742.099 ± 0.697%
P_{out}	[Pa]	1197	2859.63 ± 0.624%	17172.08 ± 2.484%	89741.29 ± 0.715%	65954.31 ± 0.229%	27071.99 ± 3.494%
ρ_{out}	[kg/m³]	0.018410	0.034 ± 0.628%	0.10489 ± 2.131%	0.30229 ± 1.234%	0.24263 ± 0.900%	0.128487 ± 1.883%
a_{out}	[m/s]	301.6748	344.887 ± 0.111%	481.24 ± 0.702%	647.98 ± 0.261%	620.13 ± 0.200%	546.05 ± 0.341%
u_{out}	[m/s]	2111.7240	2081.42 ± 0.159%	1940.85 ± 0.078%	1693.17 ± 0.716%	1736.37 ± 0.269%	1856.58 ± 0.502%
μ_1	[°]	-	-	-	-	22.6107	20.9405
μ_2	[°]	-	-	-	-	20.939	17.2536

3.2 Results of Theoretical-Numerical Simulation.

The software *Paraview* is the viewer of results. One can seen the results of the theoretical-numerical simulation, the distribution of thermodynamic properties along the body of the vehicle flying under the design conditions. Comparing the results of the CFD simulation with the results of the theoretical-numerical analysis can be said that the results are within the expected. It is presented as contour curves of Mach number (Fig. 8), pressure (Fig. 9), temperature (Fig. 10) and fluid density (Fig. 11) along the vehicle:

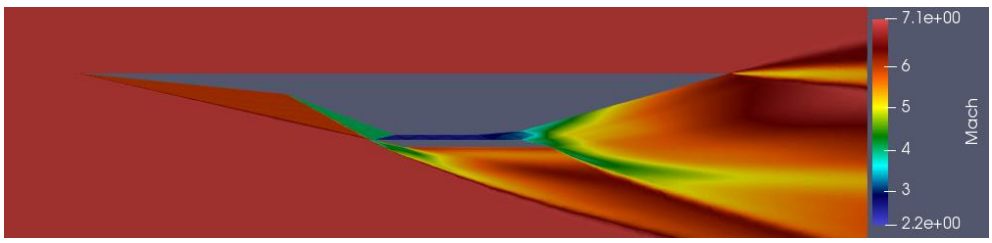

Figure 8. Contour Curve of the Mach Number.

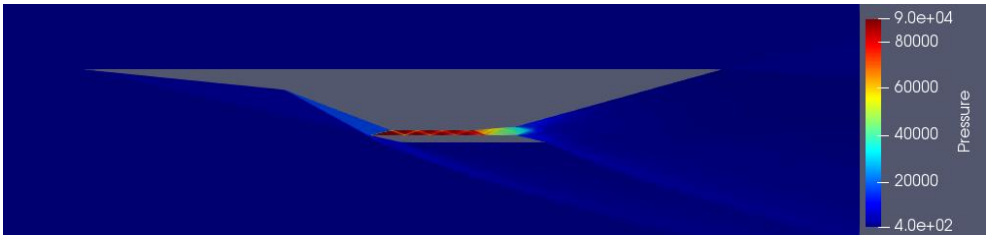

Figure 9. Contour Curve of the Pressure.

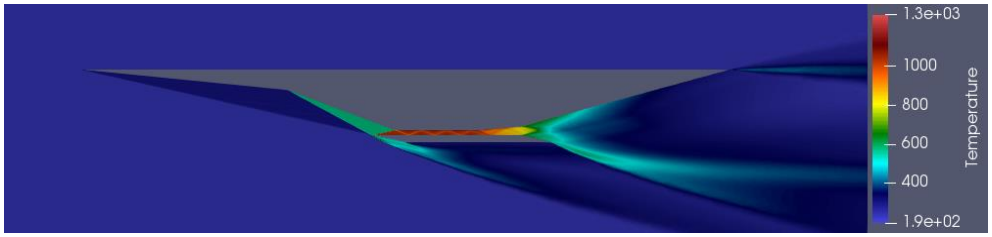

Figure 10. Contour Curve of the Temperature.

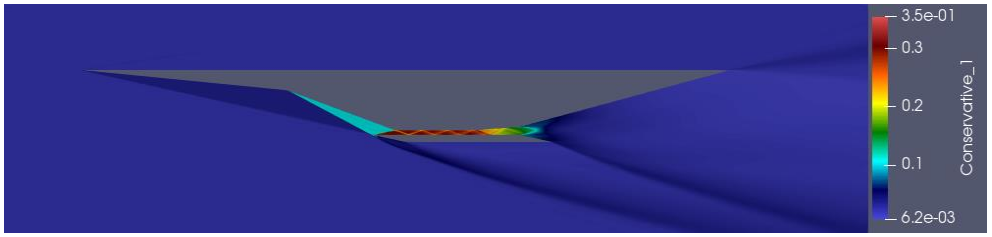

Figure 11. Contour Curve of the Density.

4. CONCLUSIONS

It is concluded that the software "SU²_CFD" is able to perform theoretical-numerical simulation of the flight of hypersonic vehicles considering permanent airflow, adiabatic (without heat exchange), non-viscous (without boundary layer) effect, and calorically perfect gas (without real gas effects).

The results obtained by the theoretical-numerical simulation are similar to those obtained by theoretical-analytical analysis.

It is still necessary to compare the results obtained by the software "SU² CFD" with those obtained by "ANSYS Fluent" in other research works developed at the IEAv.

5. ACKNOWLEDGEMENTS

The authors thank their advisors, Dr. Heidi Korzenowski; Dr. Paulo Gilberto de Paula Toro and Dr. Israel da Silveira Rêgo for their commitment for passing on their knowledge of aerothermodynamics and hypersonics to students and for encouraging students to research and improve their learning during undergraduation. Our deep gratitude to the Brazilian Ministry of Defense, who has helped us financially through the IEAv budget project, where the authors are scholarship holders. The Students will be eternally grateful to each one who has helped to accomplish this work.

6. REFERENCES

Anderson Jr., J. D. 2003. *Modern Compressible Flow*. New York: McGraw-Hill.

Heiser, W. H., Pratt, D. T. 1994. *Hypersonic Airbreathing Propulsion. Washington* D.C.: AIAA - American Institute of Aeronautics and Astronautics.

Nasa. 1976. *U.S standart atmosphere 1976*. Washington, DC.

Carvalhal, A. K. *Simulação Numérica da Aerodinâmica do Demonstrador Tecnológico SCRamjet 14-X B*. 2015. Master's dissertation in the post-graduate program in Science and space technologies, in the area of spatial propulsion concentration and hypersonic – Instituto Tecnológico de Aeronáutica, São José dos Campos.

7. RESPONSIBILITY NOTICE

The author(s) is (are) the only responsible for the printed material included in this paper.